

# Investigation of the flow around an aircraft wing of section NACA 2412 utilising ANSYS fluent

Rob IVES\*<sup>1</sup>, (Andrew) Stewart KEIR<sup>1</sup>, Edet BASSEY<sup>1</sup>, Faik A. HAMAD<sup>1</sup>

\*Corresponding author

<sup>1</sup>School of Science & Engineering, Teesside University,  
Middlesbrough, TS1 3BA, UK  
M2084041@live.tees.ac.uk\*, N3085595@live.tees.ac.uk,  
M2233300@live.tees.ac.uk, F.Hamad.tees.ac.uk

DOI: 10.13111/2066-8201.2018.10.1.10

Received: 20 November 2017/ Accepted: 28 January 2018/ Published: March 2018

Copyright © 2018. Published by INCAS. This is an “open access” article under the CC BY-NC-ND license (<http://creativecommons.org/licenses/by-nc-nd/4.0/>)

*Aerospace Europe CEAS 2017 Conference,*

*16<sup>th</sup>-20<sup>th</sup> October 2017, Palace of the Parliament, Bucharest, Romania*  
*Technical session & Workshop Aerothermodynamics & Thermal Science*

**Abstract:** *The aim of this paper is to produce and validate a simulated model of the external flow around the NACA 2412 using ANSYS Fluent; utilising experimental data for a low velocity case (20.73 m/s) from literature. This model will be subsequently used to produce data for a high velocity case (272.1 m/s, Mach = 0.8) which is the practical velocity for commercial aircraft. Both an infinite aspect ratio wing (2D) and a finite aspect ratio wing (3D) will be the subjects of this investigation. Experimental data on which the simulated models will be compared and hence validated is taken from Jacobs et al. [1]. This experimental data contains both a finite aspect ratio wing and an infinite aspect ratio wing. An accurate simulation model of the external flow around a wing will be beneficial in the visualisation of the flow; particularly in the investigation of the onset of a stall and the aerodynamic characteristic differences between the wing root and wing tip. The model will also provide simulated data of an external flow condition of which no experimental data currently exists. Finally, value will be gained in the investigation between the differences of an external flow around a 2-dimensional (2D) wing versus a 3-dimensional (3D) wing. All simulations exhibited flow physics consistent with those seen in experimental data; further validating the results. A detailed methodology has been provided with a view that new data becomes available for this aerofoil and wing geometry. Considering the aerofoil simulation, incredible accuracy has been achieved. However, with regards to the wing simulation, further work is required to identify the issue which resulted in a lower lift curve slope when compared to the experimental data.*

**Key Words:** *CFD simulation, finite wing, lift coefficient, drag coefficient, pressure coefficient*

## 1. INTRODUCTION

A 2D wing is an aerofoil of infinite span with identical span-wise location and flow. When considering a 3D wing with finite span, span-wise flow differences and vortices are introduced by the presence of the wingtips. A wing generates upward lift due to span-wise pressure difference between its upper and lower surface which diminishes at the wingtips. Consequently, circulatory motion is formed about the wingtip and develops into vortices which travel downstream of the trailing edge with a downward velocity field. The wingtip vortex induces downwash with increased momentum since the airflow is forced down by the lifting wing, which results in increased drag [2]. The 3D wing effective Angle of Attack

(AoA) is less than the 2D wing angle of attack due to the presence of downwash and induced angle on the 3D wing. Thus, the lift generated by a 3D wing is lower than that of the 2D wing. To increase the lift, the 3D wing must operate at a greater angle of attack  $\alpha$  in order to generate as much lift as the 2D wing.

The purpose of this paper is threefold. The first is to use experimental data from literature [1, 3] to validate a CFD model for an infinite aspect-ratio wing (2-D wing). With respect to the finite aspect-ratio wing (3D wing), CFD results will be compared with the experiment from Jacobs, et al. [1] and the recent data produced by Prabhakar and Ohri [4]. The second is to use the validated models to produce data for lift and drag coefficients at high velocity (272.1 m/s, Mach = 0.8) which is the velocity of commercial aircraft. The third purpose is to produce new data for pressure distribution at different locations along the span to illustrate and confirm the three-dimensional flow around the wing within CFD. The NACA 2412 was chosen for this study as experimental data exists in literature, which can therefore be used for the validation of the CFD model; the NACA 2412 was used on the Cessna 150 [2]. The knowledge and experience developed in this paper will be used in studying the aerodynamic performance of small aircraft; a build project to be undertaken by an aerospace group at Teesside university in next two years.

## 2. COMPUTATIONAL DOMAIN GEOMETRY

The computational flow domain must be subdivided into a series of elements to form a structured mesh; the topology of this mesh can be that of “C”, “O” or “H”. Both Eleni, et al. [3] and Liu & Qin [5] utilise a C-type grid topology to mesh and subsequently analyse an external flow surrounding an aerofoil; neither source provide justification. Khare, et al. [6] also utilises a C-type grid topology in the analysis of aerofoils; however, provide sound justification stating that a c-type grid has the capability to “capture the wake flow region very well when compared” to other grid topologies as a result of the geometry.

Eleni, et al. [3] describe a domain height of 20 chord lengths in the analysis of an aerofoil. Liu & Qin [5] concur that a far-field boundary located at a distance of 20 chords is appropriate and shows that the outlet must also be positioned 20 chords from the aerofoil. Thus, in both the 2D and 3D domain, the far-field, inlet and outlet boundary is placed 20 chord lengths from the leading edge of the wing. In the 3D case, the domain is revolved  $180^\circ$  about the horizontal axis; creating the symmetric boundary condition wall.

## 3. METHODOLOGY

### 3.1 General simulation set up

The general set-up within ANSYS of the infinite aspect ratio wing and the finite aspect ratio wing are generally aided by Richards, et al. [7] and Mullen [8] as well as Veronica [9] respectively. The Density-based solver was selected due to the flow compressibility. The viscous model is considered and the appropriate turbulence model is selected. Velocity inlet is used as inlet boundary condition and pressure outlet for the outlet boundary.

### 3.2 Mesh independence study

Both the 2D and 3D mesh is continually refined, alongside a grid independence study, until the solutions can be termed “grid independent”. Figures 1 & 2 show the change in lift coefficient for three different values of grid number.

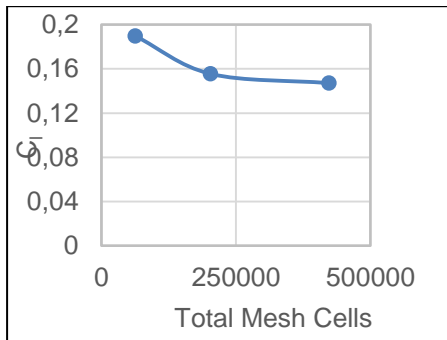


Figure 1: 2D Mesh Independence Study

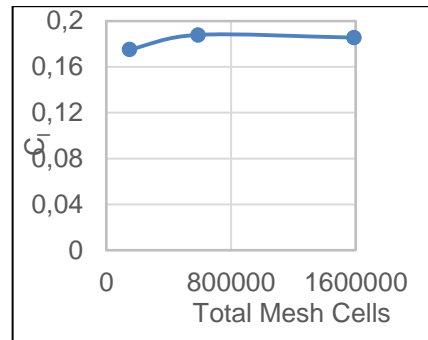
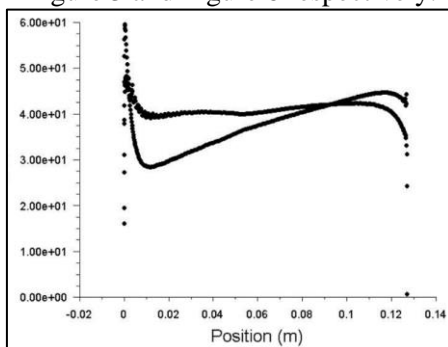
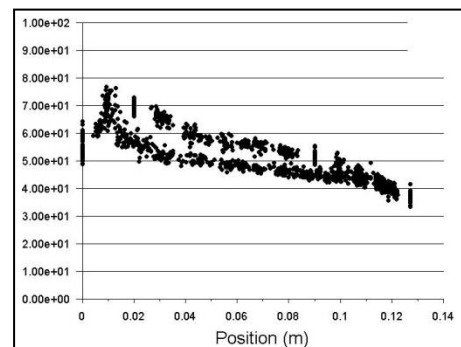


Figure 2: 3D Mesh Independence Study

### 3.3 Maximum first layer height $y^+$

The non-dimensional cell wall distance parameter, or  $y^+$ , defines the distance from a wall to a certain cell height as a function of the properties of the flow. Eleni, et al. [3] utilises a maximum  $y^+$  value of 0.2 whereas Liu & Qin [5] utilise a value of 0.7 in the analysis of aerofoils. In summary, Khare et al.[6] state that the value of  $y^+$  must be less than 1 thus avoiding the requirement for wall functions which “generally over predict the viscous drag in comparison”. However, to achieve a first layer height  $y^+$  value of approximately one, particularly when computing the solution considering the greater velocity, would be infeasible. The level of refinement would require resources over and above that which is available. ANSYS has the capability to refine a mesh automatically. However, this too would be inappropriate as the refinement would change the mesh of each solution differently as a result of the angle of attack. Hence each solution could no longer be assumed with confidence to be grid independent. Hence a compromise is used, whereby a maximum  $y^+$  value of 30 - 300 is achieved and used in conjunction with standard wall functions as recommended [10]. Figures 3 – 6 present the  $y^+$  values for the aerofoil and wing at low velocity (20.73 m/s) and high velocity (272.1 m/s). The results are within the acceptable range of 30 -300 for all cases. With regards to the flow of higher velocity, the mesh must be refined as a result of a significant velocity increase. This was completed by increasing the bias factor and reducing the maximum thickness parameter of the inflation layers of the 2D and 3D mesh respectively. Despite a change in the mesh, the solution can still be termed grid independent as the quantity of nodes was not affected. Further to this, the  $Y^+$  values of the flows were ensured to be as similar as possible. This can be seen for the aerofoil and wing within Figure 3 and Figure 6 respectively.

Figure 3:  $Y^+$  against chord length (aerofoil: 20.73 m/s)Figure 4:  $Y^+$  against chord length (Wing: 20.73 m/s)

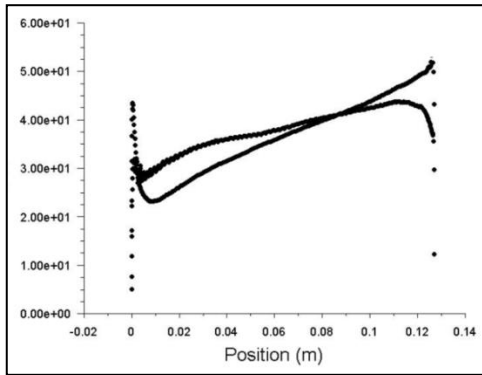


Figure 5:  $Y^+$  against chord length (aerofoil: 272 m/s)

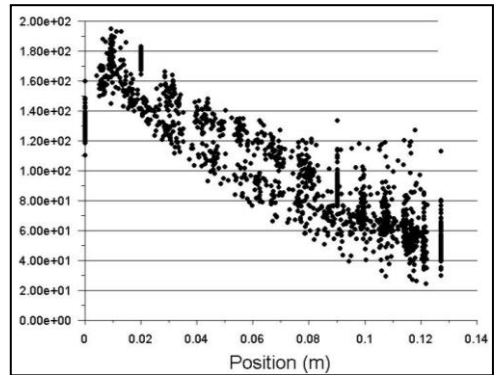


Figure 6:  $Y^+$  against chord length (Wing: 272 m/s)

## 4. FLOW DOMAIN PHYSICS

### 4.1 Flow properties

The velocity of the airflow is selected to be 20.73 m/s as defined by Jacobs, et al. [1]. With a view to extending data regarding the NACA 2412, a second velocity of 272.1 m/s is selected of which no experimental data exists. The resulting Reynolds Number ( $Re$ ) of each flow will be 3,250,000 and 42,660,250 respectively.

### 4.2 Turbulence models

Four turbulence models are selected for analysis. These models include, Spalart-Allmaras, K-epsilon, K-Omega SST and finally Reynolds Stress model. As discussed above, standard wall functions will be utilised with models which permit their use; these include RSM and K-epsilon.

The lift and drag coefficients of the simulations will be compared to experimental data over a wide range of AoA to determine the most accurate model. Figures 7 & 8 present the comparison of experimental data with predictions from different turbulence modules.

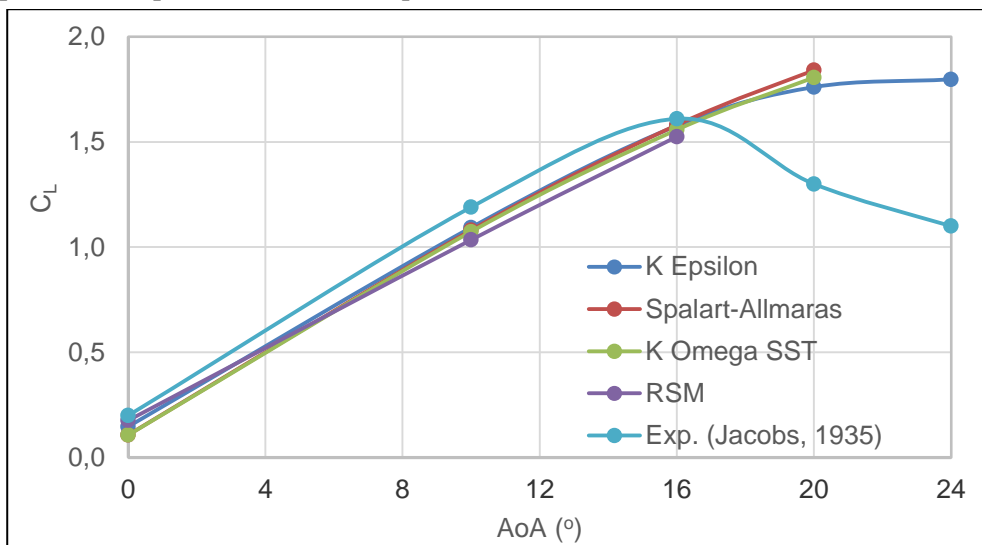


Figure 7: Lift Coefficient against AoA – Aerofoil (20.73 m/s)

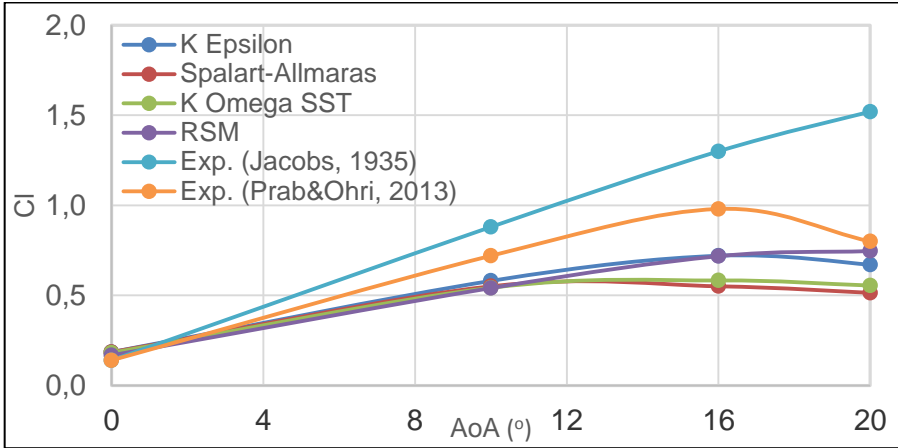


Figure 8: Lift Coefficient against AoA – Wing (20.73 m/s)

### 5. RESULTS AND DISCUSSION

#### 5.1 Comparison of aerofoil lift and drag coefficient with wing

The lift and drag coefficient values of the aerofoil and wing generated within ANSYS at a velocity of 20.73 m/s are now compared against experimental data. The 3D wing effective angle of attack is less than the 2D wing angle of attack due to the presence of downwash and induced angle on the 3D wing. A comparison is made between the lift and drag coefficients of the 2D infinite and 3D finite wing flow as shown in Figures 9 and 10 respectively. The lift coefficient is calculated by the integration of the values on the wing surface. The lift generated by the 2D aerofoil was higher than that of the 3D wing. The increase in drag coefficient for wing flow is associated with decreased lift. This behaviour is caused by the generation of vortices, downwash and a very turbulent region of wake at the trailing edge. The 2D wing showed stall characteristics which signified the location of boundary layer separation and turbulence at AoA around 16°.

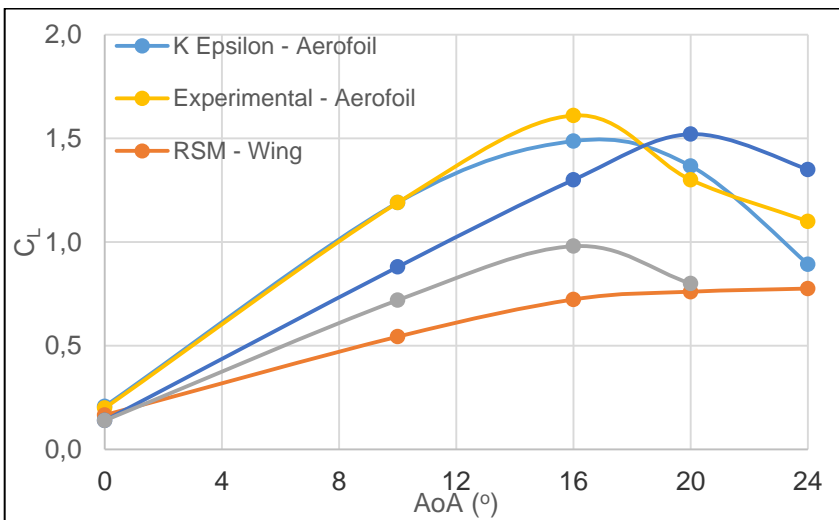


Figure 9: Lift Coefficient against AoA – 20.73 m/s

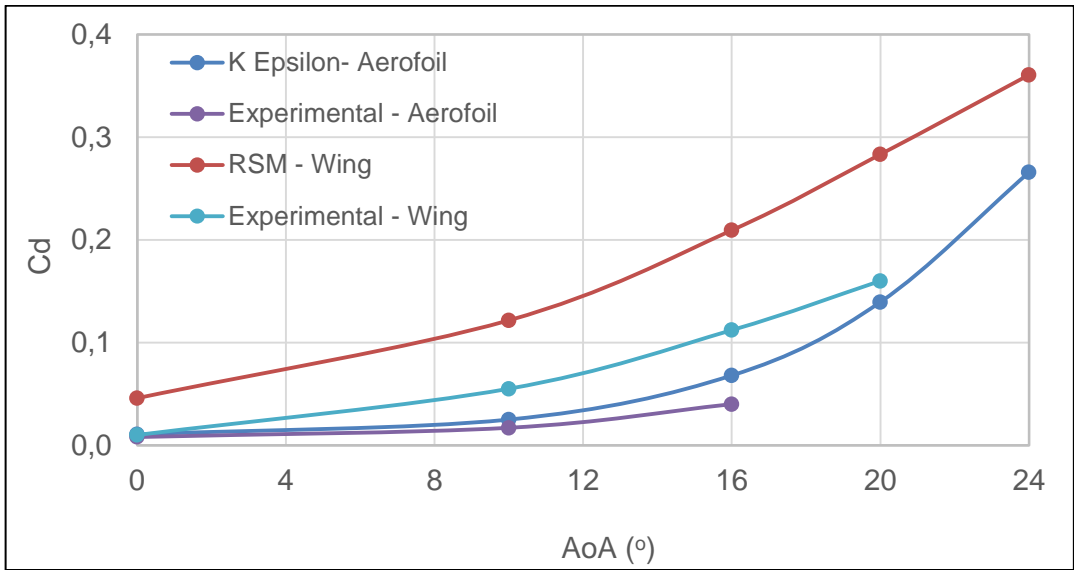


Figure 10: Profile Drag Coefficient against AoA – 20.73 m/s

### 5.2 Effect of free stream velocity on lift and drag coefficients

Having compared the results of simulation to the real world experimental data and commenting on their validity, further tests can now be completed to expand the data available for the NACA 2412. Figure 11 illustrates the profile lift coefficient calculated by ANSYS for a NACA 2412 aerofoil and wing of the same section for Mach = 0.8 (272.1 m/s) flow. Figure 12 illustrates the profile drag coefficient of the wing and aerofoil for Mach = 0.8 (272.1 m/s) flow.

The data for 20.73 m/s are also included to show the effect of free stream velocity (Mach number) on lift and drag coefficients.

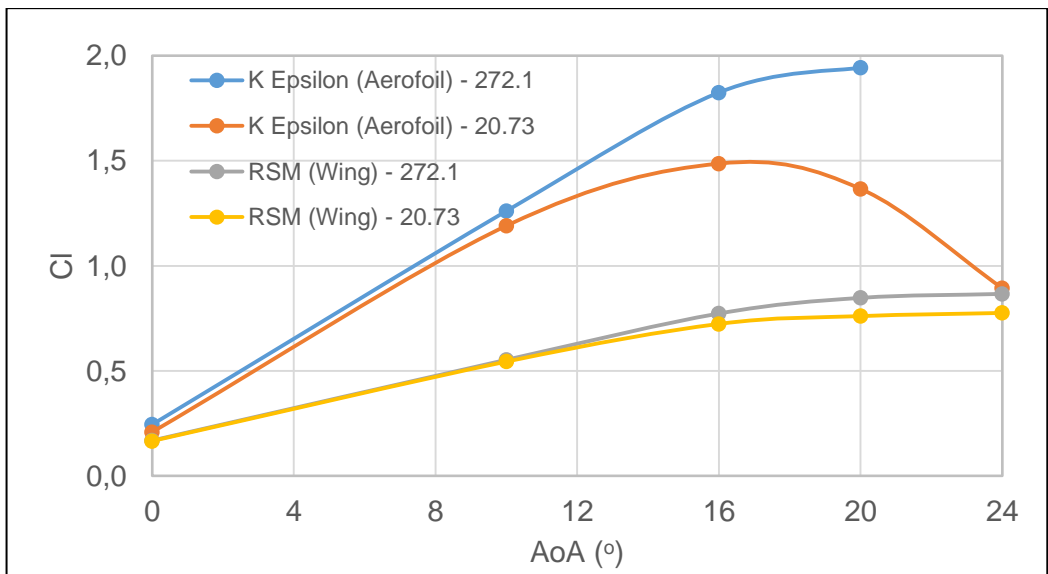


Figure 11: Lift Coefficient against AoA for 20.73 and 272.1 m/s

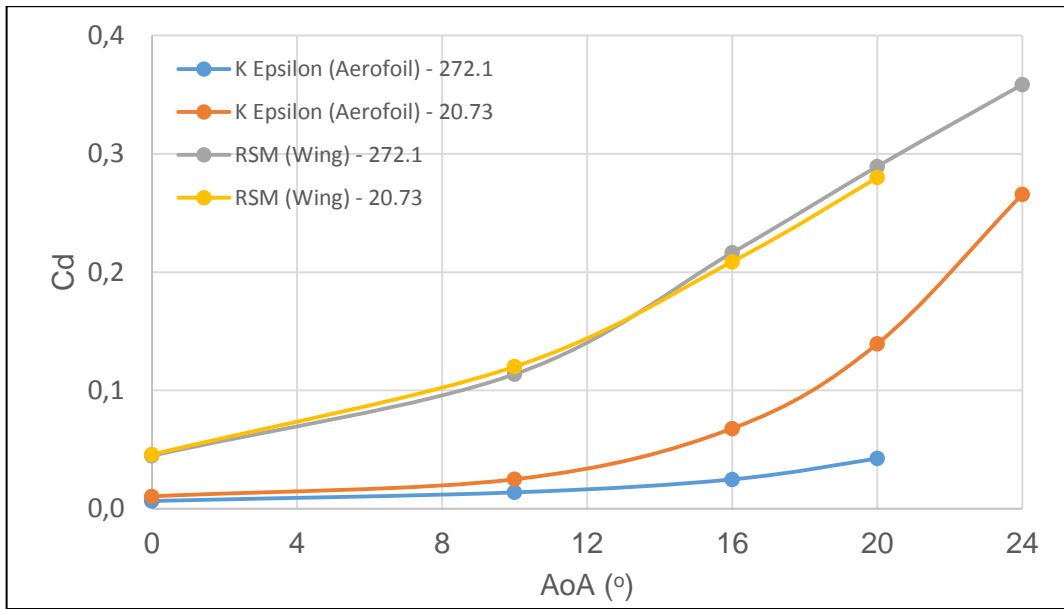


Figure 12: Profile Drag Coefficient against AoA – 272.1 m/s

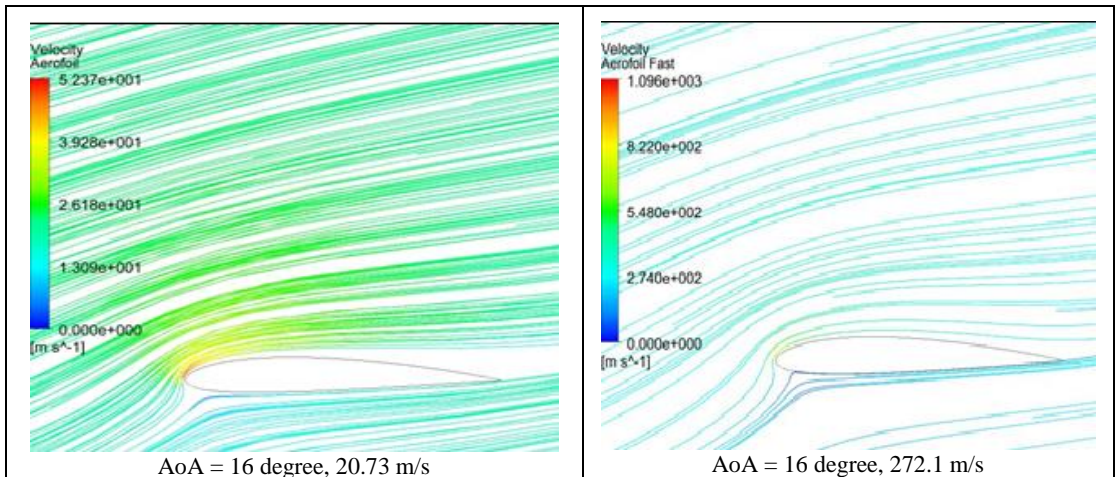
### 5.3 Velocity streamline plot

The streamlines contours in Figure 13 show the flow around the aerofoil at the two flow stream velocities for different angles of attack.

The noticeable difference between the lift and drag coefficients for the aerofoil can be explained by the significant difference in flow separation at low velocity compared to high velocity.

The results also show that this becomes more significant at higher angle of attack. It can be observed from the images in Figure 13 that as the Reynolds number of the flow increases, the flow remains attached to the aerofoil at greater angles of attack.

This leads to a greater stall angle and a higher maximum lift coefficient. For instance, it can be clearly seen that the flow has separated at 20 degrees AoA in a 20.73 m/s flow; however, at 272.1 m/s the flow remains mainly attached.



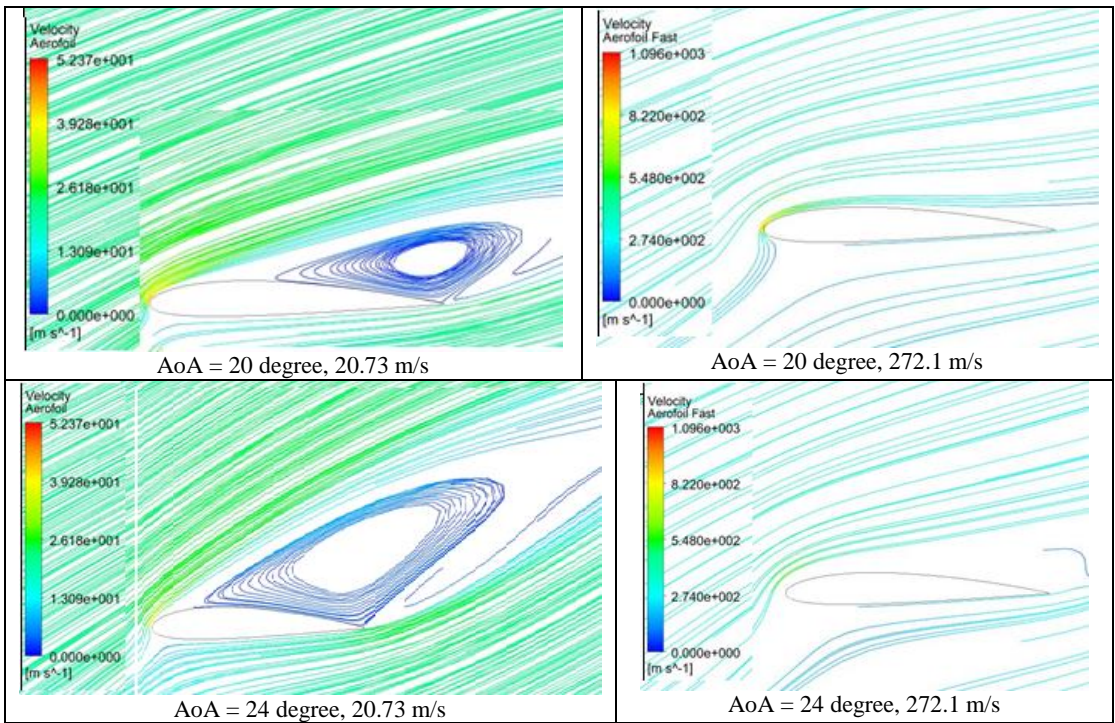
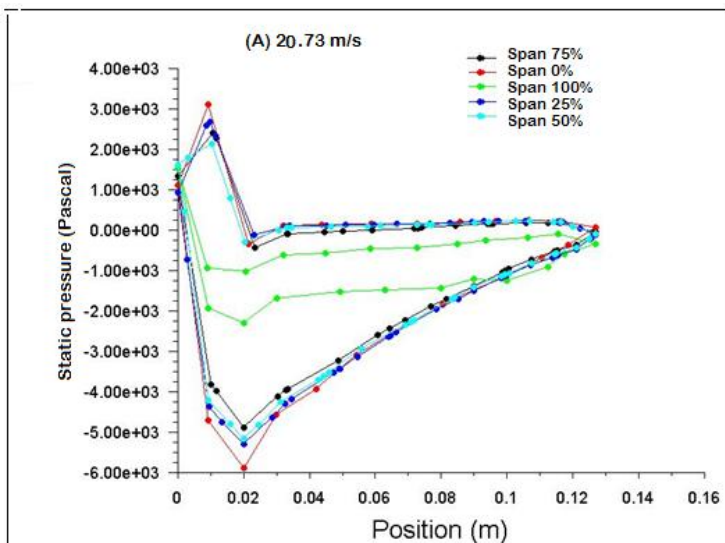


Figure 13: The effect of AoA on streamline contours

### 5.4 Static pressure

The following two plots show the static pressure distribution on the surface of the wing at various positions along the span at 20.73 m/s and 272.1 m/s respectively (Figure 14). It can be noted within Figure 14 that the differential in static pressure between the top surface and the bottom surface of the wing decreases as the plot changes from 0% (symmetry) to 100% (tip of the wing). This is a result of the high pressure under the wing travelling around the tip of the wing to the lower pressure on the top surface of the wing.





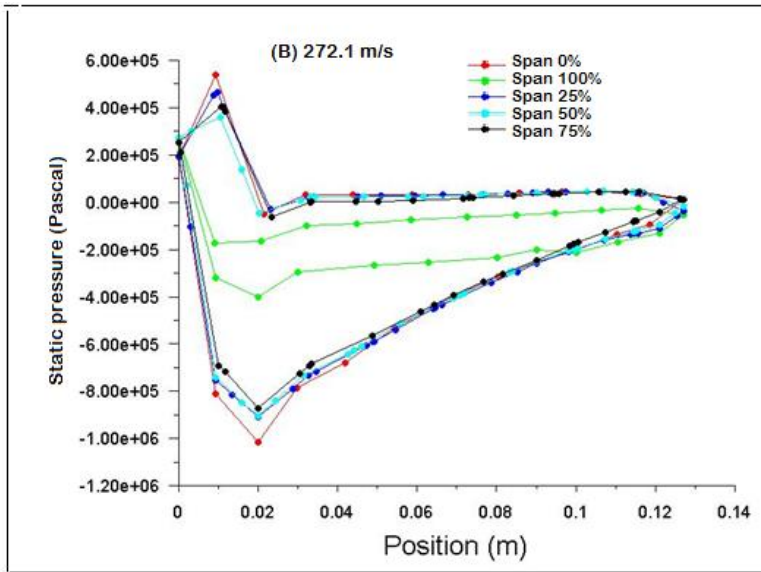


Figure 14: Static pressure plot along span of wing at 10 dDegreesAoA.  
A) 20.73 m/s and B) 272.1 m/s

## 6. CONCLUSIONS

The flow around the NACA 2412 aerofoil and wing was studied using Ansys Fluent 17.1. The investigation includes two parts: i) to validate the CFD model with experimental data from literature; ii) to use the model to produce new data at  $M = 0.8$  for lift coefficient, drag coefficient and pressure distribution on the wing at different span locations. The main conclusions are:

1. For 20.73 m/s, the results show that prediction from all the turbulence modules at low angles of attack below  $16^\circ$  for the aerofoil compared well with experimental data. On the other hand, the prediction from all turbulence model are less than the two sets of experimental data from literature references and the discrepancies increase for higher angles of attack. The results show that  $k-\epsilon$  is appropriate for aerofoil simulation while RSM is the best turbulence model for wing simulation. The results show the predicted drag coefficient from  $K-\epsilon$  model in good agreement with experimental data. However, the data predicted from RSM for the wing is higher than experimental data.
2. The results from the model show no significant effect of free stream velocity on lift and drag coefficients for the wing. The aerofoil experiences an increase in the lift coefficient and decrease in drag coefficient at high velocity (272.1 m/s) compared to low velocity (20.73 m/s).
3. The difference between the lift and drag coefficients for the aerofoil can be explained by the appearance of separation at lower angle of attack for low velocity compared to high velocity.
4. The simulation produced very interesting results for pressure distribution at different locations along the span. The lower static pressure distribution near the wing tip compared to the root confirm the three-dimensional flow around the wing.

---

**REFERENCES**

- [1] E. Jacobs, K. Ward and R. Pinkerton, *Report No. 460: The Characteristics of 78 Related Airfoil Sections From Tests In The Variable-Density Wind Tunnel*, National Advisory Committee For Aeronautics. p. 14., Washington, D.C., 1935.
- [2] J. Anderson, *Fundamentals of Aerodynamics*, 5th ed., New York: McGraw-Hill. p. 20, 2010.
- [3] D. Eleni, T. Athanasios and M. Dionissios, Evaluation of the turbulence models for the simulation of the flow over a National Advisory Committee for Aeronautics (NACA) 0012 airfoil, *Mechanical Engineering Research*, vol. 4, no. 3, pp. 100-111, 2012.
- [4] A. Prabhakar and A. Ohri, CFD analysis on MAV NACA 2412 wing in high lift take-off configuration for enhanced lift generation, *Journal of Aeronautical and Aerospace Engineering*, 2013.
- [5] S. Liu and N. Qin, Modelling Roughness Effects for Transitional Low Reynolds Number Aerofoil Flows, *Aerospace Engineering*, vol. 229, no. 2, pp. 280-289, 2014.
- [6] A. Khare, A. Singh and K. Nokam, Best Practices in Grid Generation for CFD Applications Using HyperMesh, *Computational Research Laboratories*, pp. 2, 3, 5.
- [7] S. Richards, K. Martin and J. Cimbala, *ANSYS Workbench Tutorial - Flow Over an Airfoil [PDF]*, 17 January 2011. [Online]. Available:  
[http://www.mne.psu.edu/cimbala/Learning/ANSYS/Workbench\\_Tutorial\\_Airfoil.pdf](http://www.mne.psu.edu/cimbala/Learning/ANSYS/Workbench_Tutorial_Airfoil.pdf). p. 7.[Accessed 02 October 2016].
- [8] B. Mullen, *FLUENT - Flow over an Airfoil*, 2014, [Online]. Available:  
<https://confluence.cornell.edu/display/SIMULATION/FLUENT+++Flow+over+an+Airfoil>. [Accessed 02 October 2016].
- [9] A. Veronica, *Fluent - 3D Transonic Flow Over a Wing*, 2015. [Online]. Available:  
<https://confluence.cornell.edu/display/SIMULATION/FLUENT+++3D+Transonic+Flow+Over+a+Wing>. [Accessed 12 October 2016].
- [10] \* \* \* ANSYS, *Modeling Turbulent Flows [PDF]*, December 2006. [Online]. Available:  
[http://www.southampton.ac.uk/~nwb/lectures/GoodPracticeCFD/Articles/Turbulence\\_Notes\\_Fluent-v6.3.06.pdf](http://www.southampton.ac.uk/~nwb/lectures/GoodPracticeCFD/Articles/Turbulence_Notes_Fluent-v6.3.06.pdf). pp. 6-17.[Accessed 10 December 2016].